Unveiling SparkLink Low Energy: A Comparative Measurement Study

BOYA LIU, The Hong Kong University of Science and Technology, Hong Kong, Hong Kong
ZHENYU REN, The Hong Kong University of Science and Technology, Hong Kong, Hong Kong
YANBO ZHANG, The Hong Kong University of Science and Technology, Hong Kong, Hong Kong
MO LI, The Hong Kong University of Science and Technology, Hong Kong, Hong Kong
JIAXIN LIANG, Huawei Technologies Co Ltd, Shenzhen, China
BIN HE, Huawei Technologies Co Ltd, Shenzhen, China
JIE LI, Huawei Technologies Co Ltd, Shenzhen, China
HAO WU, Huawei Technologies Co Ltd, Shenzhen, China
JINGBIN ZHOU, Huawei Technologies Co Ltd, Shenzhen, China

SparkLink Low Energy (SLE) is a new short-range wireless communication technology designed to satisfy the increasing demands of future short-range scenarios. While SLE promises fundamental improvements over traditional Bluetooth, a thorough real-world evaluation is lacking. This article provides a detailed evaluation framework that includes access layer benchmarking and end-to-end application validation, presenting the first comprehensive comparison between SLE and traditional Bluetooth technologies. Benchmarking reveals SLE offers a 4× increase in data rate, a 3.84× reduction in latency, and a 10 dB improvement in sensitivity. To evaluate SLE against actual application QoS requirements, we implement an end-to-end evaluation system for validation across three practical application scenarios. Based on experimentation and parameter analysis, we propose a design for QoS-centered optimization. These results underscore SLE's fundamental advancements over Bluetooth and its potential in real-world applications, offering insights for further optimization of this communication technology.

CCS Concepts: • **Networks** → **Link-layer protocols**; **Network measurement**; • **Hardware** → **Power and energy**; **Board- and system-level test;**

Additional Key Words and Phrases: Wireless communication, sparklink low energy

Boya Liu and Zhenyu Ren contributed equally to this research.
This research is supported in part by the internal fund of Hong Kong University of Science and Technology, Hong Kong, and in part by Hong Kong GRF 16204224.
Authors' Contact Information: Boya Liu, The Hong Kong University of Science and Technology, Hong Kong, Hong Kong; e-mail: bliuby@connect.ust.hk; Zhenyu Ren, The Hong Kong University of Science and Technology, Hong Kong, Hong Kong; e-mail: zrenax@connect.ust.hk; Yanbo Zhang (corresponding author), The Hong Kong University of Science and Technology, Hong Kong, Hong Kong; e-mail: yanbozhang@ust.hk; Mo Li, The Hong Kong University of Science and Technology, Hong Kong, Hong Kong; e-mail: lim@cse.ust.hk; Jiaxin Liang, Huawei Technologies Co Ltd, Shenzhen, Guangdong, China; e-mail: jiaxin.liang@huawei.com; Bin He, Huawei Technologies Co Ltd, Shenzhen, Guangdong, China; e-mail: hebin17@huawei.com; Jie Li, Huawei Technologies Co Ltd, Shenzhen, Guangdong, China; e-mail: leo.lijie@huawei.com; Hao Wu, Huawei Technologies Co Ltd, Shenzhen, Guangdong, China; e-mail: wuhao82@huawei.com; Jingbin Zhou, Huawei Technologies Co Ltd, Shenzhen, Guangdong, China; e-mail: zhoujingbin@huawei.com.



This work is licensed under a Creative Commons Attribution 4.0 International License.

© 2026 Copyright held by the owner/author(s).
ACM 2577-6207/2026/01-ART6
https://doi.org/10.1145/3776559

ACM Reference Format:
Boya Liu, Zhenyu Ren, Yanbo Zhang, Mo Li, Jiaxin Liang, Bin He, Jie Li, Hao Wu, and Jingbin Zhou. 2026. Unveiling SparkLink Low Energy: A Comparative Measurement Study. *ACM Trans. Internet Things* 7, 1, Article 6 (January 2026), 24 pages. https://doi.org/10.1145/3776559

1 Introduction

The rapid evolution of the **Internet of Things** (**IoT**) has driven the emergence of advanced short-range applications, such as industrial automation, smart homes, and intelligent vehicles, which impose stringent **Quality of Service** (**QoS**) requirements on communication technologies. These requirements include high throughput, minimal latency, exceptional reliability and ultra-low power consumption [15]. For instance, real-time audio streaming demands an effective throughput exceeding 4 Mbps with latency below 10 milliseconds [37], while industrial sensor monitoring requires a packet loss rate of less than 0.001%. However, existing short-range communication technologies, particularly **Bluetooth Low Energy** (**BLE**), face significant performance bottlenecks in meeting these demands due to inherent limitations in their protocol stack architecture.

At the physical layer, BLE's low bandwidth and GFSK modulation limit its data rate to 2 Mbps, with practical efficiency further reduced by overhead, interference, and the tradeoff between reliability and speed introduced by Forward Error Correction [35, 40]. At the link layer, the minimum connection interval of 7.5 ms increases end-to-end latency and reduces efficiency, as upper-layer data must wait for the next interval to transmit [27]. Moreover, BLE's inability in dynamic QoS adaptation restricts its suitability for certain applications [35], while the absence of cross-layer coordination often results in unnecessary compromises in certain performance aspects. These constraints also make it challenging to perform further optimizations based on the traditional architecture of BLE.

To better serve emerging short-range applications, the International SparkLink Alliance introduced **SparkLink Low Energy** (**SLE**) technology in 2022 [1]. SLE aims at overcoming the performance bottlenecks of traditional Bluetooth [1]in scenarios demanding low power consumption, high throughput, low latency, and high reliability. While SLE initially promised notable enhancements in all these aspects, a thorough evaluation of its performance is lacking. In this article, our aim is to fill this gap and experimentally evaluate the performance improvements of SLE over traditional Bluetooth in practical applications.

In its core, SLE leverages a cross-layer QoS coordination mechanism and a highly flexible access layer design, as illustrated in Figure 1. At the physical layer, SLE supports bandwidth options of 1 MHz, 2 MHz, and 4 MHz, along with efficient technologies such as PSK modulation and polar code, significantly enhancing spectral efficiency and interference resilience. At the link layer, SLE incorporates multiple link types – connectionless data links, asynchronous data links, and synchronous data links – designed for device discovery, reliable data transmission, and low-latency high-speed communication, respectively. At the basic service layer, SLE includes a QoS management module that dynamically selects link types and configures transmission parameters based on application requirements.

To validate the effectiveness of such cross-layer design, this article conducts a comprehensive benchmarking of SLE's practical performance in terms of throughput, latency, reliability, and power consumption, and highlights its performance improvements through comparison with BLE. Specifically, we aim to: (1) quantify SLE's performance under different physical and link layer parameter configurations; (2) evaluate SLE's capability to meet the diverse QoS requirements of various applications.

[1]Bluetooth referes to both Bluetooth Classic and Bluetooth Low Energy (BLE) unless otherwise specified.

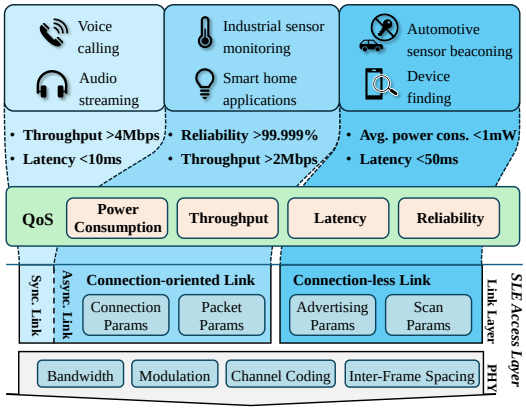


Fig. 1. SLE's flexible access layer effectively satisfies the varied QoS demands of real-world applications [7, 15, 37].

We design the measurement methodology based on two principles: *comprehensiveness* and *completeness*. On one hand, we designed a set of evaluation metrics to comprehensively assess various QoS performance aspects under different protocol stack parameter configurations and environmental conditions. On the other hand, our experimental design aims at providing a complete, bottom-up demonstration of SLE's improvements than BLE across all layers of the protocol stack. This includes technical enhancements at the physical layer (e.g., improved channel coding schemes and upgraded chipset capabilities), parameter optimizations at the link layer (e.g., connection interval adjustments and data link matching), and QoS coordination at the service layer.

Our measurement demonstrates that SLE provides a 4× higher data rate, a 3.84× decrease in communication latency, and a 10 dB improvement in sensitivity compared to traditional Bluetooth. End-to-end use case studies confirm SLE's capability to meet diverse QoS needs. The contributions of this article are as follows:

— We conduct the first real-world experimental benchmarking of SLE's performance, comprehensively verifying its capabilities in communication throughput, latency, reliability, and power consumption.
— We provide a comparative analysis of SLE against BLE across all four performance aspects, involving over a hundred parameter combinations across different layers, demonstrating SLE's significant improvements than BLE.
— We validate SLE's practical performance in meeting diverse QoS requirements by constructing end-to-end tests for three application scenarios.
— We propose an innovative optimization algorithm based on experimental observations and adapt it into SLE's QoS optimization framework, further enhancing its optimization capabilities.

The article is structured as follows: Section 2 outlines the core mechanisms of SLE, BLE and classic Bluetooth. Section 3 describes the experimental methodology. Section 4 compares SLE and BLE's performance. Section 5 presents three case studies. Section 6 proposes a parameter optimization model. Section 7 reviews related work, and Section 8 concludes the article.

2 Background

This section introduces the connection-oriented and connection-less approaches in SLE and BLE, highlighting their primary distinctions. **Bluetooth Classic** (**BT**) is also briefly mentioned to contrast its characteristics with SLE and BLE.

Table 1. PHY Parameter Options of SLE and BLE

Parameter	BLE	SLE
Operating Band	2.4GHz	2.4GHz/5.1GHz/5.8GHz
Bandwidth	1MHz/2MHz	1MHz/2MHz/4MHz
Modulation Scheme	GFSK (1 bit/Sym)	FT1: GFSK (1 bit/Sym) FT2: PSK (2 bits/Sym)
Channel Coding	LE 1M/2M PHY: None LE Coded PHY: FEC	FT1: None FT2: Polar code

(5.1/5.8 GHz is not available on commercial products currently. FT: Frame Type.)

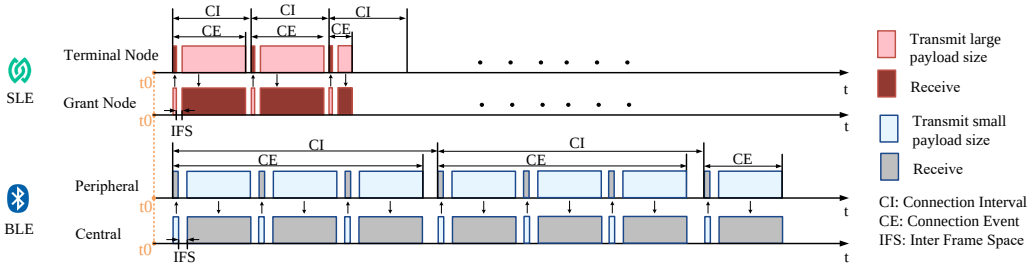


Fig. 2. Packet exchange flow of connection-oriented mechanism in SLE and BLE. Here, *Transmit large payload size* refers to the case where SLE, enabled by its high PHY rate, can transmit, *e.g.*, one 1370-byte packet within a 2.5 ms CI. In contrast, *Transmit small payload size* denotes the case for BLE, which, due to its lower PHY rate, can only deliver, *e.g.*, three 244-byte packets within a 10 ms CI.

2.1 SLE and BLE

2.1.1 Overview of SLE. Similar to BLE, SLE supports the same channel map and bandwidth options of 1 MHz and 2 MHz. In addition, SLE offers an extra 4 MHz bandwidth mode, in which the channel structure is different: it adopts a channel spacing of 4 MHz, resulting in a total of 20 channels, each with a bandwidth of 4 MHz [2]. Furthermore, SLE provides other configurable physical layer parameters, such as modulation schemes and channel coding, as summarized in Table 1.

2.1.2 Connection-oriented Communication. As depicted in Figure 2, the flow of packet exchanges within connection-oriented communication mechanisms is shown for both SLE [2] and BLE [35]. In this scenario, two linked devices—termed *Grant* and *Terminal* in SLE (*Central* and *Peripheral* in BLE terminology)—communicate by exchanging data within non-overlapping time periods, referred to as ***Connection Events*** **(CEs)**. For both SLE and BLE, each CE starts with a packet sent by the grant. If the terminal receives this packet, it responds after an ***Inter Frame Space*** **(IFS)**. The time between the start of two successive CEs defines the ***connection interval*** **(CI)**. To save power, the terminal device typically remains in a sleep state, periodically awakening to check for any transmissions from the grant.

Although operating in similar flow, SLE outperforms BLE in several aspects: First, SLE is designed to support a lower minimum CI of 1.25 ms (versus 7.5 ms for BLE), which helps balance throughput and latency for a better user experience. Second, SLE permits longer packet transmissions, improving efficiency by amortizing protocol overhead (e.g., headers and redundancy from channel coding) across larger payload. Third, SLE achieves a smaller IFS (125 μs, 150 μs for BLE), made possible by improved chip capabilities in Tx-Rx switching, which also further reduces latency and increases

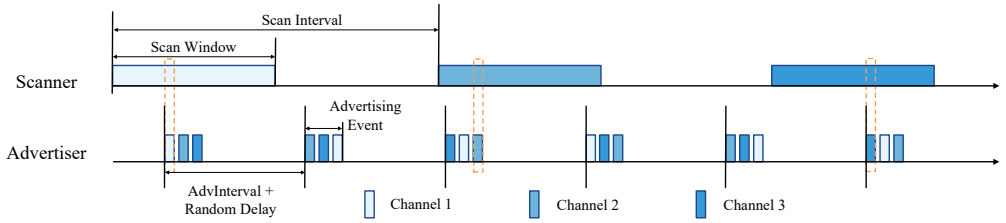


Fig. 3. Illustration of connectionless communication process for SLE and BLE.

throughput. In addition, in its **physical layer** (**PHY**), SLE supports wider bandwidth, more efficient modulation, and advanced channel coding schemes to provide higher throughput and better reliability. Table 1 compares the parameter options of the PHY for SLE and BLE.

2.1.3 Connectionless Communication. Connectionless data transmission allows nearby devices to exchange information without an established session. An *advertiser* broadcasts data packets via *advertising*, which allowing other devices to receive this information without establishing a connection, while nearby devices, called *scanners*, listen on a specific channel to intercept them. Figure 3 shows that during an *advertising event*, the advertiser sends packets over three channels in a random sequence. Successive advertising events are separated by an interval and a random delay to reduce collisions. Simultaneously, the scanner listens on one of the channels for a periodic *scan window* according to the *scan interval*. The scanner captures the packet if its active scan window matches the event in time and frequency. This mechanism also aids in device discovery and connection establishment. SLE employs an advertising scheme similar to BLE, utilizing three primary advertising channels (37, 38, and 39) to minimize interference from Wi-Fi and other 2.4 GHz devices. Notably, SLE allows shorter advertising intervals (minimum 4ms) than BLE (minimum 20ms), offering higher throughput and lower latency.

2.2 Bluetooth Classic

Bluetooth Classic operates in the 2.4 GHz ISM band using **Gaussian Frequency Shift Keying** (**GFSK**) for Basic Rate and $\pi/4$-DQPSK, 8DPSK for Enhanced Data Rate, supporting data rates of 1 Mb/s, 2 Mb/s, and 3 Mb/s, respectively. In this approach, communication channels are divided into time slots, each 625 μs long, with central and peripheral alternating transmission. Packets must align with slot boundaries and can span up to five time slots. Frequent POLL-NULL packet exchanges are required to maintain the connection, preventing deep-sleep state and increasing power consumption.

3 Methodology

3.1 Measurement Objectives

In order to evaluate whether SLE's enhancements (detailed in Section 2) provide satisfactory link quality in serving the emerging short-range applications, this study focuses on four key performance aspects: **energy consumption**, **throughput**, **latency**, and **reliability**. Multiple metrics will be used to evaluate each aspect, offering a comprehensive performance overview. Specifically, energy consumption will be assessed by measuring standby and transmission power through electrical current profiling. Throughput will be examined using PHY Rate, Effective PHY Rate, and Goodput. Latency will be quantified through service latency, air-time round-trip latency, and device discovery latency. Link reliability will be evaluated by analyzing the effects of RSSI, Wi-Fi interference, and SNR on Goodput and BER. Finally, by integrating these metrics across different layers and

dimensions, a comparative analysis will provide deeper insight into performance and its underlying technical factors.

3.2 Measurement Approach

The testing strategy of this study is guided by two core principles: *comprehensiveness* and *completeness* as shown in Figure 1. *Comprehensiveness* means designing multiple metrics to evaluate various QoS performance aspects, while considering the impact of different protocol stack parameter choices and diverse testing environments. *Completeness* means conducting measurements across all layers of the SLE and BLE protocol stack, from the physical layer to the service layer, to fully assess the optimization effects at each level.

Adhering to the principle of *comprehensiveness*, multiple metrics are established to evaluate performance across different dimensions. For instance, communication throughput is assessed using metrics such as PHY rate, effective PHY rate, and goodput, while latency is evaluated through metrics including service latency, air-interface round-trip latency, and device discovery latency (refer to Section 4 for detailed definitions). *Comprehensiveness* also involves evaluating the impact of various protocol parameters, as well as their combinations. Specifically, the study examines seven categories of protocol parameters, including bandwidth, frame types (which determine modulation and channel coding schemes), connection interval, payload length, advertising interval, and scan duty cycle. Moreover, this principle emphasizes assessing the impact of environmental variations, which is achieved by incorporating four experimental settings: a corridor, an office, an RF shielding room without interference, and one with controlled interference.

Following the principle of *completeness*, our experimental design aims at providing a complete, bottom-up demonstration of SLE's improvements than BLE across all layers of the protocol stack. This includes enhancements at the physical layer, such as expanded communication bandwidth, improved channel coding, and upgraded chip hardware; optimizations at the link layer, such as connection interval adjustments and data link matching; and QoS negotiation at the service layer. To isolate and analyze the impact of specific design improvements, we employ a controlled variable approach in iterative testing and precisely quantify the enhancements by defining a set of evaluation metrics at different stack layers. Furthermore, to reflect the combined effects of SLE's cross-layer co-design, we designed and conducted three case studies based on typical applications. These case studies demonstrate the practical performance of the SLE protocol stack in meeting diverse QoS requirements for various applications.

3.3 Experiment Hardware

The SparkLink Alliance has introduced multiple chips supporting the SLE protocol, notably the widely used Hi3863V100 [20] and Hi2821V100 [21]. Our measurements employ two development boards with these chips for SLE experiment testing. Details of these boards are provided below:

- Nearlink-DK-WS63E: Based on the Hi3863V100 multi-mode SoC and the FBB-WS63 SDK [20], this development board offers software interfaces that allow configuration of a wide range of physical- and link-layer parameters, including bandwidth, modulation schemes, and connection intervals. Such flexibility makes it particularly suitable for fine-grained experimental control. The board features a high-performance 32-bit microprocessor with 606 KB of SRAM and 4 MB of Flash memory, operating at a clock speed of 40 MHz. In addition to SLE, the Hi3863V100 system protocol stack also integrates Wi-Fi and BLE, offering multi-mode capabilities.
- BearPi-Pico H2821: Powered by the Hi2821V100 chipset and the FBB-BS2X SDK [21], this board integrates a high-performance 32-bit microprocessor with 160 KB of SRAM and 512 KB of Flash memory. It runs at a clock frequency of 64 MHz. Notably, Hi2821V100 chipset

supports running custom system protocol stacks, enabling the operation of either the SLE or BLE stack individually, as well as a single substack on either the central or peripheral side.

The use of different platforms aligns with these principles, ensuring that for each metric, the most suitable hardware is used to faithfully capture performance. Specifically, in our experiment, we mainly use Nearlink-DK-WS63E to test SLE's communication performance, benefiting from its flexible software interfaces. Nevertheless, its integration of multiple protocol stacks makes it challenging to precisely measure the power consumption of an individual protocol like SLE or BLE. To address this, we employ BearPi-Pico H2821 as a complementary device, which supports a single protocol stack compilation and runtime environment, accurately reflecting the power usage of that protocol.

Throughout the measurement, we also tested the performance of BLE and BT to provide reference. The experiments were conducted using the following two boards, respectively:

— Nordic nRF52840 DK: A common BLE development board based on the nRF52840 chip, it supports Bluetooth 5.0 and includes interfaces from the Nordic nRF5 SDK [33]. This board features a 32-bit ARM Cortex-M4 CPU running at 64 MHz, with 256 KB of RAM and 1 MB of Flash memory.
— ESP32 DevKitC v4: Produced by Espressif, this compact board features the ESP32 chip and supports Bluetooth 4.2 (Classic and BLE) with ESP-IDF interfaces [12]. This board is built around the ESP32-D0WDQ6 chip, which features a dual-core 32-bit LX6 microprocessor running at up to 240 MHz, with 520 KB of SRAM and 4 MB of Flash memory.

4 Performance Evaluation

In this section, we evaluate the performance of SLE in comparison with BLE and BT across four key aspects: energy consumption, throughput, latency, and reliability. Each of these aspects is analyzed in a dedicated subsection, based on controlled measurements conducted in both shielding room and real-world scenarios. For each performance metric, we first describe the experimental setup, including parameter selection, device requirements, and testing scenarios. We then present the experimental results and provide further analysis of the performance metric.

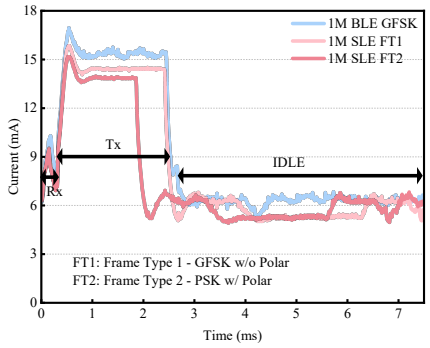
4.1 Energy Consumption

Energy consumption plays a crucial role in IoT applications, especially for devices with limited energy supplies. Here, we examine SLE's power consumption through run-time current measurements and compare these results with BLE to demonstrate the performance discrepancies.

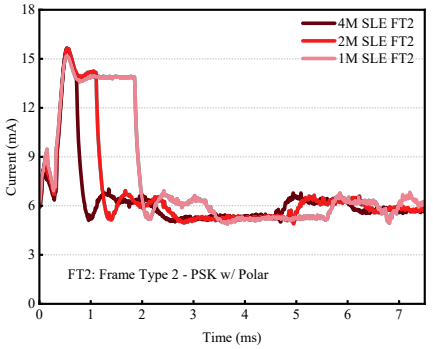
4.1.1 Experiment Setup. We assess the instantaneous run-time current for every operational phase of both SLE and BLE, spanning Radio Active Tx, Radio Active Rx, and Radio IDLE, within a single connection interval. For both SLE and BLE protocols, the service data length is consistently set at 244 bytes (ATT_MTU defined in Bluetooth specification [35]) and the CI at 7.5 ms during the assessment of power efficiency. Multiple variables such as protocol type, bandwidth, and device role are accounted for in the evaluation. Specifically:

— We evaluate the impact of various modulation schemes of the SLE and BLE while maintaining a bandwidth of 1MHz.
— We examine the effect of bandwidth on SLE using its Frame Type 2 parameter settings (See Table 2).
— We conduct multiple experiments to analyze distinctions when the device is either transmitting or receiving.

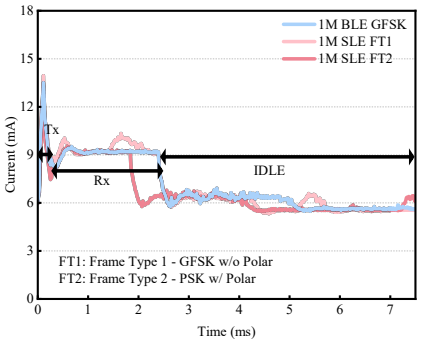
We employed the BearPi-Pico H2821 evaluation board for hardware characterization. To eliminate interference from other protocols, we individually flashed dedicated peripheral and central firmware



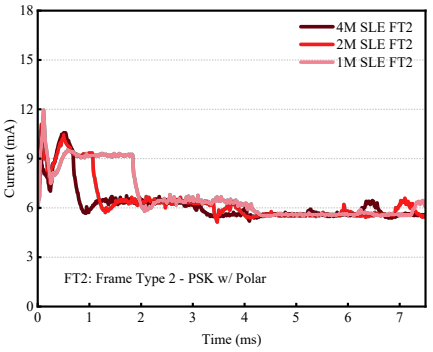
(a) SLE v.s. BLE, with varied modulation and coding schemes (peripheral side)



(b) SLE profiling with different bandwidth settings (peripheral side)



(c) SLE v.s. BLE, with varied modulaton and coding scheme (central side)



(d) SLE profiling with different bandwidth settings (central side)

Fig. 4. Electric current usage of SLE and BLE at a transmit power of 6 dBm. In settings (a) - (d), SLE consistently demonstrates lower or equal power consumption throughout the entire CI. (Hereafter, "w/o Polar" indicates operation without polar coding and "w/ Polar" indicates operation with polar coding.).

for SLE and BLE, respectively. A constant 3.3 V supply was provided, and current consumption during CI was measured using a precision power monitor. The transmit power was configured to 6 dBm.

4.1.2 Experiment Results. Figure 4(a)–(b) and (c)–(d) illustrate the current profiles when the device functions as a peripheral/terminal and a central/grant, respectively. In Figure 4(a) and (c), we annotate the three communication stages within one CI.

Comparing the measurements between SLE and BLE under the same bandwidth of 1 MHz (Figure 4(a) and (c)), SLE consumes consistently less current than BLE (as in Figure 4(a)) or a comparable amount (as in Figure 4(c)) during both the Radio active (Tx/Rx) and Radio idle stages. Table 2 outlines the differences in detail. Note that the current draw values in Table 2 are measured within different radio states, and different data rates and configurations only lead to different durations of these states, not the current draw values themselves. Beyond lower instantaneous power usage, SLE's more efficient modulation and coding shortens radio active time, further reducing the total energy consumption. Higher-order modulation schemes can transmit more bits per symbol, allowing the same amount of data to be sent in a shorter time. This leads to reduced transmission duration, which in turn decreases the overall radio active time.

Table 2. Average Current in Different Stages of SLE and BLE

Current of Stages	BLE GFSK	SLE FT1	SLE FT2
Radio Active Tx (mA)	14.59	13.47	13.85
Radio Active Rx (mA)	9.52	7.88	8.43
Radio IDLE (mA)	6.34	5.74	5.25

The current of SLE is similar to BLE in each stage.

On the other hand, when examining the impact of SLE's increased bandwidth (Figure 4(b) and (d)), it can be observed that higher bandwidth does not raise current for a peripheral/terminal node and slightly ups peak current for a central/grand node. Yet, the significantly reduced radio active duration due to increased bandwidth ultimately decreases total energy cost.

Due to hardware limitations, we could not evaluate Bluetooth Classic in the same manner as SLE and BLE. Therefore, we referred to published references for its current consumption values. Bluetooth classic offers high throughput but consumes more power than BLE [18, 23, 29] due to its need for continuous connection maintenance by sending control messages even without data transfer. Measurements show BT's peak current hits 40 mA and stays around 13.51 mA in sleep mode, about 2.88 times higher than BLE, aligning with our results.

4.2 Throughput

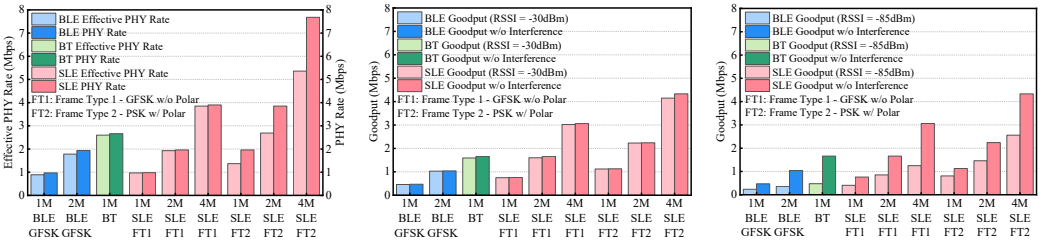
This section compares the data rates of BLE, BT, and SLE at their physical and application layer, assessing the impact of various parameter settings and environmental conditions.

4.2.1 Evaluation Metrics. We use the following metrics to quantify the performance of BLE, BT, and SLE:

- Effective PHY Rate: This metric characterizes the actual transmission rate of useful **service data unit** (**SDU**) at the upper layer. It is calculated as the length of the SDU divided by the total airtime of the entire PHY frame, which includes PHY headers, CRC, channel coding redundancy, and pilot symbols ((one pilot symbol for every 16 data symbols). Thus, Effective PHY Rate reflects how efficiently the airtime is used for carrying application-relevant data.
- PHY Rate: This metric represents the raw transmission rate of the PHY layer payload, including coding redundancy and pilot symbols. It is calculated as the length of the PHY layer payload after modulation and coding divided by its corresponding transmission duration. In practice, the PHY Rate is always higher than the Effective PHY Rate, because the latter additionally discounts framing and signaling overhead (e.g., headers, CRC).
- Goodput: This metric quantifies the actual reception rate of service data at the application layer, reflecting the overall effectiveness of specific protocol designs, including channel coding schemes and link layer retransmission mechanisms. This metric is obtained through direct measurement at the application layer of the receiver.

4.2.2 Experiment Setup. For effective PHY rate, the packet airtime is located and extracted by signal processing techniques according to the electric current (as in Section 4.1) measured by power monitor. To determine the PHY rate, the transmission time of the data payload at the physical layer is obtained by subtracting the theoretical transmission time of PHY frame overhead (e.g., frame header and CRC) from the total packet airtime. For goodput, it is measured at three environments: shielding room (interference-free condition), office (RSSI=-30 dBm), corridor (RSSI=-85 dBm) (refer to Figure 9(a)).

Several parameters are accounted for in the evaluation, including CI, **bandwidth** (**BW**), **modulation coding scheme** (**MCS**), and packet length for both BLE and SLE. Specifically, the payload



(a) Effective PHY Rate and PHY Rate (b) Goodput (RSSI=-30dBm) (c) Goodput (RSSI=-85dBm)

Fig. 5. Comparison of physical layer data rates and application layer goodput, with considering the impact of various parameter settings and environmental conditions.

length is consistently set at the maximum values of 244 bytes for BLE and 1370 bytes for SLE. To reach the extreme data rate, the shortest CI capable of transmitting the full-length packet is utilized. For BLE, we set the CI to closely match SLE FT1 under the same bandwidth settings, maximizing data rate while maintaining similar latency. Due to different step sizes (0.125 ms for SLE versus 1.25 ms for BLE), the chosen CIs are not precisely the same. Following the order of the x-axis in Figure 5(a), the CIs for BLE and SLE under various parameter configurations are 12.5 ms, 7.5 ms, 11.75 ms, 6.125 ms, 3.375 ms, 8.5 ms, 4.5 ms, and 2.5 ms, respectively.

We employed the Nearlink-DK-WS63E for SLE, the nRF52840 DK for BLE, and the ESP32 DevKit C v4 for BT (Section 3.2). To measure the three aforementioned metrics for BLE, SLE, and BT under varying BW and MCS settings, experiments are conducted in both an office environment and a shielding room. We measure the average data rate for every 100 MB of transmitted data, repeating each measurement 200 times to minimize random errors.

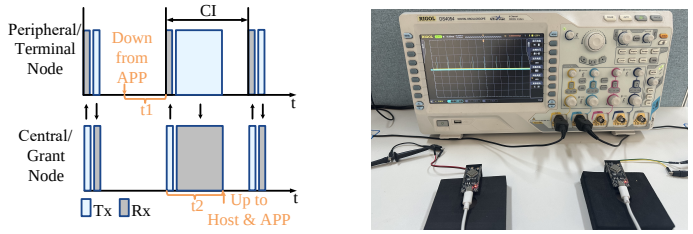
4.2.3 Experiment Results. Figure 5(a) and (b)–(c) illustrate the data rate of physical layer and application layer with different PHY configurations, signal conditions (e.g., RSSI), and interference scenarios (e.g., shielded environments and offices) of BLE, BT, and SLE.

As shown in Figure 5(a), SLE achieves its highest PHY rate at 7.68 Mbps (4 MHz bandwidth, FT2), which is 3.96 × higher than BLE's peak rate of 1.94 Mbps and 2.89 × that of BT. The results demonstrate the efficacy of SLE's broader BW and more advanced modulation scheme.

The gap between the effective PHY rate and PHY rate mainly accounts for the effect of physical layer redundancy induced to the different techniques. This gap is significantly larger in SLE FT2-based communication, which requires additional redundancy such as polar codes for improved noise and interference tolerance (refer to Section 4.4) and pilot symbols at various densities for accurate phase estimation, both essential for PSK demodulation. Nonetheless, even with this overhead, SLE's maximum effective PHY rate is still 3.01 × that of BLE and 2.02 × that of BT.

Comparing across Figure 5(a) and (b), SLE with FT2 gains 115.4% enhancement over BLE in goodput (interference-free condition), significantly higher than the 51.2% improvements in effective PHY Rate. This is primarily attributed to two differences in link-layer mechanisms: First, SLE permits a maximum payload length of 1370 bytes, significantly larger than BLE's 244 bytes. This larger payload spreads protocol overhead (e.g., packet header) across more data, thereby reducing overhead per effective byte. Second, SLE allows a higher duty cycle, which results from its shorter CI and IFS, thereby minimizing idle time between connection events.

Figure 5(b) compares the goodput between BLE, BT, and SLE at an environment with high RSSI level (-30 dBm). SLE achieves 4.15 Mbps, which is 4.03 × higher than that of BLE and 2.61 × higher than that of BT. When moving to an environment with low RSSI (Figure 5(c)), SLE with FT2 (e.g.,



(a) Illustration of service latency and air-time round-trip latency

(b) Experimental setup for latency measurement

Fig. 6. (a) Depiction of service latency and air-time round-trip latency and (b) the experimental setup for latency measurement.

2 MHz bandwidth) shows a reduction in goodput from 2.23 Mbps to 1.46 Mbps, which is only about 34%. In contrast, BLE and BT's goodput decrease by 65% and 71.4%, respectively. The comparison suggests the efficacy of the polar coding scheme adopted by SLE's PHY.

In this experiment, SLE attains higher throughput than BLE but also shows higher average current consumption across the tested configurations. For example, the measured average current for SLE falls between approximately 12.3 mA and 13.4 mA, while BLE's values are in the range of about 10.8 mA to 11.2 mA. Despite the higher current draw, SLE demonstrates lower energy consumption per transmitted bit in all tested scenarios. Specifically, the observed energy consumption per bit for SLE ranges from roughly 57.8×10^{-6} mJ/bit in the lowest-rate setting to 2.98×10^{-6} mJ/bit in the highest-rate setting, compared with about 75.3×10^{-6} mJ/bit to 10.7×10^{-6} mJ/bit for BLE. These results indicate that the higher data rate of SLE offsets its slightly higher current consumption, leading to improved energy efficiency on a per-bit basis.

4.3 Latency

4.3.1 Experiment Metrics. The following metrics are used to quantify the performance of BLE and SLE:

— Service latency: This metric characterizes the end-to-end latency of service data, defined as the time interval from the server's (typically the peripheral) upper-layer application sending service data to the client's (typically the central) host fully receiving that data ($t_1 + t_2$ in Figure 6(a)). Note that the client-server model is typically used in the application layer during the process of service discovery and interaction, while the central-peripheral model is used in the link layer during the process of connection establishment.
— Air-time round-trip latency: This metric represents the air time of packet interaction, defined as the time to complete a full-length packet interaction between the central and the peripheral (t_2 in Figure 6(a)).
— Device discovery latency: This metric quantifies the time needed to find nearby devices, defined as the time from the scanner initiating its scan until the advertising packet's detection (as in Figure 3).

4.3.2 Experiment Setup.

Service Latency. Several parameters such as CI, MCS are accounted for in the evaluation. Specifically:

— We examine the impact of various connection intervals of SLE and BLE while maintaining a bandwidth of 2 MHz and modulation scheme of GFSK. The CIs of BLE are selected from

Table 3. Scanning Parameters for Device Discovery Latency Measurement

Scan Duty Cycle	SLE Scan Window (ms)	BLE Scan Window (ms)
10%	6.25-6.75	13.75-18.75
25%	11.75-12.25	27.5-32.5
100%	47.75-48.25	117.5-122.5

three representative values: the minimum CI, and the default CI used in Android [25] and iOS [3]. The CIs of SLE are computed by adding the same number of steps to its minimum CI for fairness.
— We evaluate the effect of bandwidth and MCS of SLE and BLE while maintaining a CI at 7.5 ms.
— We compare the minimum service latency of SLE and BLE.

To accurately measure the latency in microsecond level, an oscilloscope is used as a common time reference to capture precise timing signals from both Tx/Rx devices, maintaining time synchronization between two devices (Nearlink-DK-WS63E for SLE and nRF52840 DK for BLE), as shown in Figure 6(b).

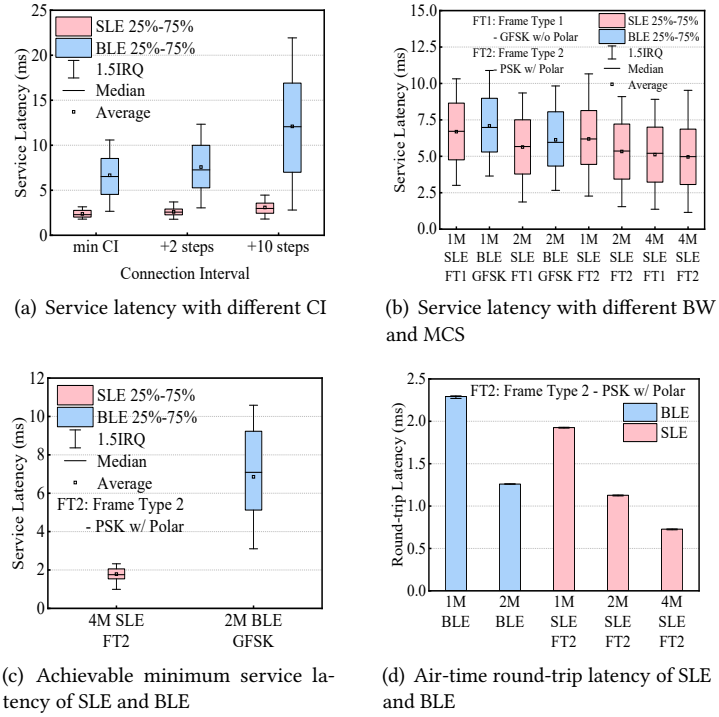
Air-time round-trip Latency. This time is located and extracted by signal processing techniques according to the electric current (as in Section 4.1) measured by the power monitor. Power monitor provides the accurate measurement of current consumption verus time, and we can extract the time duration of different radio states from the current consumption curve.

Device Discovery Latency. For both SLE and BLE, the advertising interval is consistently set at the minimum value (20 ms for BLE and 8 ms for SLE) during the assessment of device discovery latency. Scan duty cycle (i.e., the ratio between the scan window and the scan interval) is accounted for in the evaluation. Specifically, it is chosen based on three typical BLE scanner settings in the Android system of 10%, 25%, 100% [25]. We maintain a constant scan duty cycle, and enforce a fixed proportion between the scan window, scan interval, and the advertising interval. Table 3 details these specific configurations. For each duty cycle, a range of scan window and scan interval parameters are adopted with a minimum default step size: 1.25 ms for BLE and 0.125 ms for SLE. Software timestamps the start and end of each scan, enabling us to calculate the device discovery latency. For each test, a random delay of 200-220 ms is introduced to ensure randomness of scan start time.

4.3.3 *Experiment Results.*

Service Latency. Figure 7 compares the service latency of SLE and BLE, with considering the impact of CI (link layer), BW, and MCS (PHY). As the results show, SLE achieves lower service latency than BLE as CI increases by a corresponding step settings (0.125 ms and 1.25 ms) from their respective minimum CI, which equals to 1.25 ms and 7.5 ms. A shorter CI reduces the waiting time t_1 for transmitting data from the Tx buffer to the radio, as illustrated in Figure 6(a), thus leads to reduced service latency.

Figure 7(b) compares the latency by enumerating SLE and BLE's different bandwidth and modulation schemes. The wider bandwidth and higher-order modulation scheme significantly increase the data rate and naturally reduce t_2 in the service latency. Furthermore, even under the same bandwidth and MCS settings (GFSK for BLE and FT1 for SLE), SLE still achieves a lower service latency, which can be attributed to its shorter IFS.



(a) Service latency with different CI

(b) Service latency with different BW and MCS

(c) Achievable minimum service latency of SLE and BLE

(d) Air-time round-trip latency of SLE and BLE

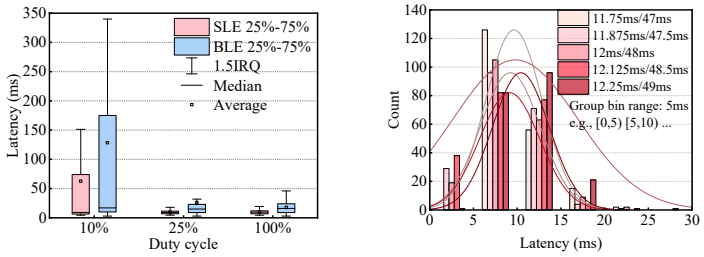
Fig. 7. Comparison of service latency and air-time round-trip latency, with considering the impact of physical layer modulation and coding schemes and link layer connection interval.

Figure 7(c) presents the minimum service latency achieved by applying the optimal parameter combinations (CI, bandwidth, and MCS) of SLE and BLE. Notably, SLE reduces the extreme service latency by 64.3% compared to BLE.

Although SLE achieves lower service latency, it generally incurs higher average current consumption than BLE under minimum-latency conditions, recording 8.15 mA for SLE (FT2 4M) and 7.62 mA for BLE (GFSK 2M). This increase is mainly attributed to a higher duty cycle. Nevertheless, SLE exhibits substantially lower energy consumption per bit, achieving $17.23 * 10^{-6}$mJ/bit compared with BLE's $96.66 * 10^{-6}$mJ/bit, highlighting its superior energy efficiency.

Air-time round-trip Latency. Figure 7(d) compares the round-trip latency of the two technologies. SLE achieves a 73% reduction in round-trip latency compared to BLE, primarily because it employs higher-order modulation, wider BW, and shorter IFS. This decrease in round-trip time directly correlates with the enhanced data transmission rate discussed in Section 4.2. On the other hand, the shorter round-trip time also reduces device power consumption, as detailed in Section 4.1.

Device Discovery Latency. Figure 8(a) shows that SLE achieves lower device discovery latency than BLE at each scan duty cycle, primarily because SLE supports a smaller advertising interval. Notably, when the scan duty cycle is 25%, the observed device discovery latency is nearly the same as at 100%. The reason is that the 25% duty cycle's scan window nearly covers the interval between successive advertising events (i.e., the advertising interval plus a random delay), which allows the discovery process to complete within the first scan in most cases. This outcome offers practical insights for configuring parameters more efficiently.



(a) Device discovery latency of SLE and BLE

(b) Distribution of SLE device discovery latency (25% duty cycle)

Fig. 8. (a) Device discovery latency and (b) latency distribution with varied scan window configurations.

To demonstrate the robustness of our parameter choices, we also examine the distribution of the measured latency under various scan configurations. Each colored bar in Figure 8(b) corresponds to a different scan window/scan interval configuration. While the absolute values of the scan window and interval vary, their ratios remain constant, i.e., they represent the same duty cycle. Thus, multiple configurations are grouped together under the same duty-cycle condition, leading to multiple colored distributions in the plot. Under the same duty cycle but different scan window selections, the latency distribution remains consistent.

4.4 Reliability

This section examines the reliability of SLE and other protocols under various PHY configurations and noise interference conditions. Specifically, we measure the goodput of SLE, BLE, and BT across different RSSI levels, and we introduce Wi-Fi interference at varying traffic loads to assess performance.

4.4.1 Experiment metrics. The following metrics are used to quantify the reliability of BLE, BT, and SLE:

— Goodput: This metric quantifies the actual reception rate of service data at the application layer (refer to Section 4.2) under various environments.

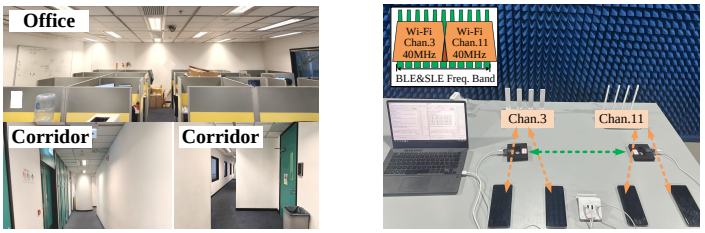
— Effective Bit Error Rate (BER_{Eff}): This metric quantifies the equivalent BER of the service data. Packet loss causes the remaining time within the CI to be idle, making BER_{Eff} an effective BER rather than the ground-truth BER. It is numerically estimated as follows [4]:

$$\begin{aligned} PRR &= \frac{Good\,put}{max\,Good\,put}, \\ BER_{Eff} &= 1 - \sqrt[PL]{PRR}, \end{aligned} \tag{1}$$

where PRR is the upper bound of the Packet Reception Rate, *max good put* is the protocol's highest achievable throughput under ideal conditions (e.g., RSSI = −30 dBm), PL is the packet length in bits.

4.4.2 Experiment Setup.

Setup of RSSI measurement. We investigate how goodput varies among different communication technologies when subjected to different RSSI levels. We fix the transmitter and move the receiver to various locations (an office or a corridor in Figure 9(a)) to obtain a different RSSI. At each location, we measure the RSSI every 30 ms and record the goodput for every 50 kB of transmitted data. Moreover, RSSI readings may vary across platforms. To ensure comparability, we calibrated BLE and



(a) Experimental environment of office and corridor

(b) Controlled interfering environment inside an RF shielding room

Fig. 9. Environments providing varied RSSI levels and interfering conditions.

SLE devices under identical conditions before experiments, confirming their RSSI values differed by less than 0.5 dBm.

Setup of Wi-Fi interference. We introduce practical Wi-Fi interference to examine its impact on BLE and SLE transmissions. We set up a controlled Wi-Fi interference source within an RF shielding room to eliminate external interference. As depicted in Figure 9(b), two Wi-Fi routers are configured on non-overlapping 40 MHz channels (ch.3 and 11) to generate interference for BLE and SLE across the full 2.402-2.480 GHz band. Three Wi-Fi interference scenarios, i.e., high load, medium load, and low load, are simulated by iPerf3 [11], with channel load information provided by phone's wifi drivers.

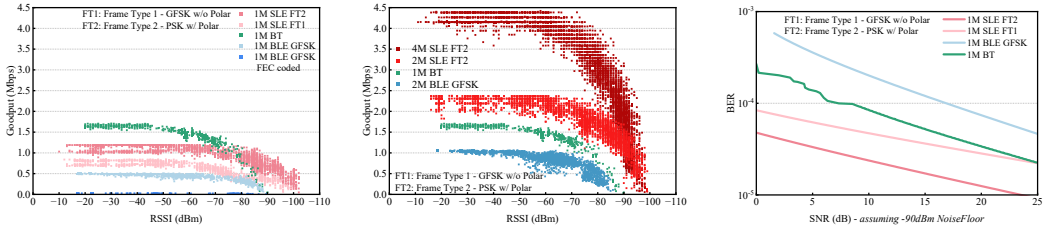
4.4.3 *Experiment Results.*

Reliability with different RSSI. Figure 10(a) compares the goodput variations of BLE, BT, and SLE over an RSSI range of -110 dBm to -20 dBm with a fixed 1 MHz bandwidth. BT's goodput drops markedly once RSSI decreases and channel conditions degrade. In contrast, SLE FT2 remains more resilient, which is mainly due to its polar-code-based interference mitigation scheme. On the other hand, SLE achieves consistently higher goodput than BLE even when the channel condition deteriorates, confirming SLE's efficacy of polar code. Figure 10(a) also compares the receiver sensitivity: SLE can maintain a receiver sensitivity of -100 dBm, which is 10 dB more resilient than BLE and BT (-90 dBm).

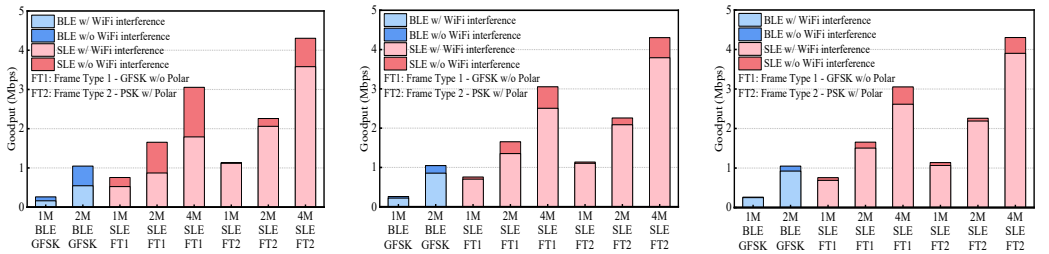
Figure 10(b) summarizes results under other PHY parameter configurations (BW, FT). Overall, SLE FT2 with 4 MHz bandwidth yields the highest goodput. Even at wider bandwidth, SLE maintains robust performance in lower RSSI environments, underscoring its superior resilience to noise.

Figure 10(c) compares the effective BER of BLE, BT, and SLE under the same bandwidth of 1 MHz. The SNR is derived from RSSI by assuming a $NoiseFloor$ of $-90dBm$ [10]. The results show that, the BER of SLE FT2 is approximately an order of magnitude lower than BLE, owing to the stronger noise-resilience capability of polar code. Even when the BW and MCS (FT1 for SLE) are the same, SLE still exhibits a lower BER than BLE, which is due to that packet loss causes the remaining duration in the CI to be idle rather than being used for data transmission. Overall, SLE's BER is lower than that of both BLE and BT.

Reliability under Wi-Fi interference. Figure 10(d)–(f) compares the anti-interference performance of SLE and BLE under different Wi-Fi traffic loads. As in Figure 10(d), SLE FT2 decreases by only 8.82% in goodput relative to the interference-free scenario (2 MHz bandwidth), significantly lower than the 47.8% drop experienced by BLE. Moreover, SLE's goodput remains high and reaches up to 6.55 × that of BLE even under high-load Wi-Fi interference. This superior performance proves the enhanced anti-interference capability provided by the polar code of SLE. Figure 10(e)



(a) Goodput under different RSSI with BW=1 MHz (b) Goodput under different RSSI and BW (c) Calculated BER with BW=1 MHz



(d) Goodput with high-load Wi-Fi interference (e) Goodput with medium-load Wi-Fi interference (f) Goodput with low-load Wi-Fi interference

Fig. 10. (a)–(c) Goodput and BER of BLE, BT, and SLE under varying RSSI levels and (d)–(f) Goodput under different levels of Wi-Fi interference.

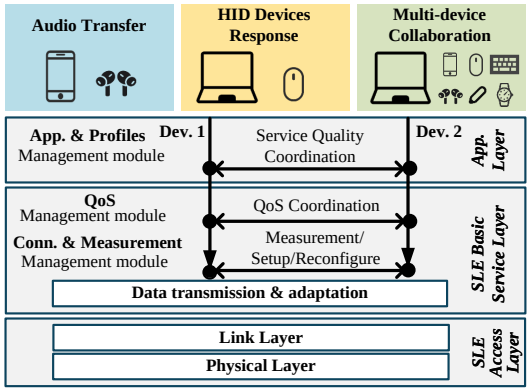
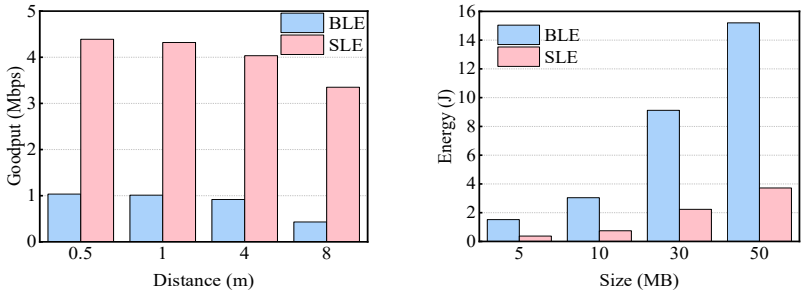


Fig. 11. Case illustration and SLE's cross-layer QoS coordination mechanism.

and (f) show analogous results under medium-load and low-load Wi-Fi interference, respectively, confirming the same overall trends.

5 Case Study

In this section, we primarily examine three practical applications: audio transfer [37], **human interface devices (HID)** response [14], and multi-device collaboration [34] as illustrated in Figure 11. Despite distinctions in QoS requirements, all upper-layer applications ultimately rely on the fundamental operations provided by the SLE access layer. Therefore, to comprehensively analyze the performance, we decompose each application into its underlying operations and



(a) Goodput at varying distances

(b) Energy when transmitting varied file sizes

Fig. 12. (a) Goodput at varying distances and (b) energy consumption when transmitting varied file sizes of SLE and BLE in an audio transfer scenario.

evaluate these operations based on the key performance aspects most relevant to each application (selected from the four aspects in Section 3.3).

5.1 Case1: Audio Transfer

Synchronous links [36] in low-power short-range communication technologies are progressively used in audio data transmission. Different from asynchronous links, which rely on unlimited link-layer retransmissions for relatively reliable transmission, synchronous links limit the retransmission numbers to maintain low latency and avoid interruptions in audio streaming. Considering the limited availability of off-the-shelf devices supporting SLE synchronous links, we emulate audio data transmission through asynchronous links under low-interference conditions.

In audio transmission applications, the key performance metrics that directly affect both audio quality are throughput and reliability. However, due to the goodput limitations of BLE, it is forced to use **Low Complexity Communication Code** (**LC3**) codec (160 kbps) to reduce the audio quality, which cannot reach **Compact Disc** (**CD**) level quality (16 bit/44.1 kHz, 1, 411.2 kbps). On the other hand, BLE's audio connections degrade in quality under crowded conditions due to increased interference and congestion on the 2.4 GHz ISM band [30], such as in subways and train stations, significantly constraining user experience.

In this case, we use two boards to mimic audio transmission between a smartphone and headphones (Figure 11) and compare the performance of SLE and BLE from three aspects: goodput at different distances, energy consumption for varied size files, and reliability among multiple concurrent links.

The results in Figure 12(a) compares the goodput of SLE and BLE under varied Tx-Rx distances of 0.5 m, 1 m, 4 m, and 8 m. BLE's relatively low data rate, ranging from several hundred kbps to around 1 Mbps, impedes the seamless transmission of high-quality audio. In contrast, SLE sustains a data rate consistently above 3 Mbps, thereby enabling the transmission of CD-level lossless audio at all tested distances.

Figure 12(b) compares the power consumption required to transmit audio files of varied sizes (5-50 MB) using SLE and BLE at a transmit power of 6 dBm. Sending 30 MB of audio data via SLE consumes approximately 2 J, which is only one-quarter of the 9 J consumed by BLE. Powered by a typical button battery (e.g., CR2032, 2376 J [32]), SLE can operate for 18 hours and transmit 35.6 GB of data, while BLE operates for 16.8 hours and transmits only 7.9 GB of data.

Figure 13(a) demonstrates our test scenario of multi-link goodput test for BLE and SLE. The results in Figure 14 show that SLE experiences a significantly smaller reduction in goodput than

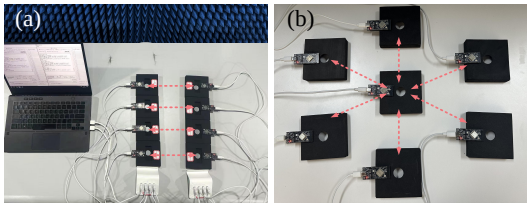
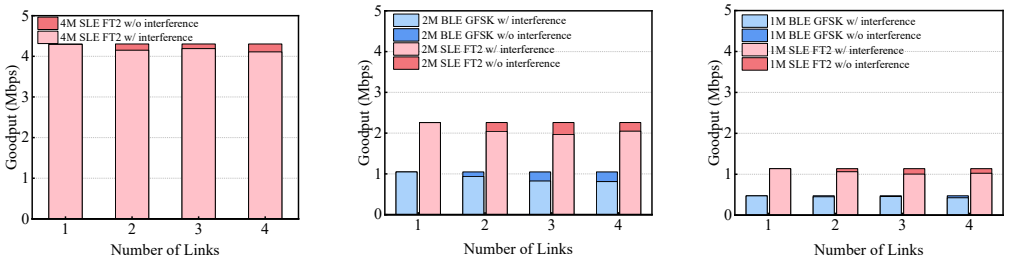


Fig. 13. Experimental setup for (a) multi-link testing of SLE and (b) 1:m testing of SLE.



(a) 4M SLE (b) 2M SLE/BLE (c) 1M SLE/BLE

Fig. 14. Average goodput of SLE and BLE multi-link testing, with different bandwidth configurations.

BLE in multi-link scenarios, ensuring more stable transmission in conditions of crowded areas like subways. Even with four simultaneous links, SLE maintains sufficiently high goodput to satisfy the requirements for stable audio.

5.2 Case2: HID Devices Response

Figure 11 illustrates a representative scenario in which a laptop interacts with a HID. The polling rate serves as a key metric indicating how frequently data are exchanged with the computer, directly influencing response speed and accuracy. In this example, we focus on the mouse, where polling rate (an application-layer metric) is closely related to service latency (a cross-layer metric detailed in Section 4.3).

Different applications put forward different QoS requirements for the polling rate of the mouse. For everyday tasks (e.g., documents, web browsing), 125-250 Hz ensures smooth performance with minimal resource usage. Video editing and casual gaming benefit from 500-1000 Hz to reduce cursor lag. Meanwhile, e-sports, 3D modeling, and VR interactions demand 2000-4000 Hz to prevent frame loss and deliver precise control and an immersive experience [26].

We evaluated SLE's performance in mouse scenarios by setting the payload length to 5 bytes, a typical value in such applications [39]. As shown in Figure 15, SLE achieves a latency of about 2.5 ms (400 Hz polling rate) based on Hi3863 chipset. Notably, a commercial mouse based on the Hi2825 chipset [19] achieves 4000 Hz [22]. In contrast, BLE exhibits around 8 ms latency (125 Hz), which is inadequate for latency-sensitive tasks such as e-sports or professional design.

5.3 Case3: Multi-device Collaboration

One-to-many device networking is increasingly important for smart terminals, connecting computers to various devices (e.g., smartphones, styluses) via wireless technologies (Figure 11), where two key operations are device discovery and one-to-many concurrent data transmission, essentially relying on connectionless and connection-oriented communication at the link layer, respectively.

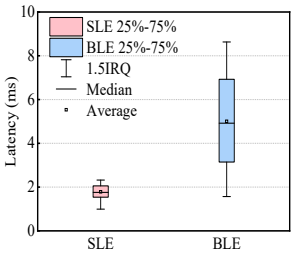
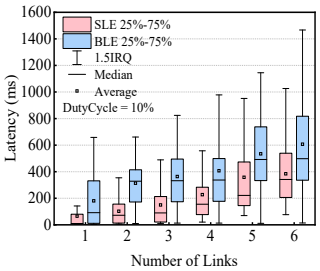
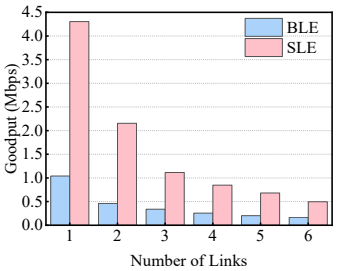


Fig. 15. Extreme service latency of SLE and BLE in HID response scenario.



(a) Device discovery latency



(b) Average goodput in 1:m communication

Fig. 16. 1:m networking and collaboration of SLE and BLE. In the 1:m scenario, one central device connects to multiple peripheral devices.

Multi-device Networking. In office settings, mobile-device networking now demands millisecond-level latency due to stringent QoS requirements. We assess networking latency of SLE and BLE by measuring the time it takes for a central device to discovery 1-6 peripherals (Figure 13(b)). We use a 10% scan duty cycle (6.5 ms/65 ms for SLE and 16.25 ms/162.5 ms for BLE) and a minimum advertising interval. The results in Figure 16(a) indicate that SLE achieves lower discovery latency, completing six-device discovery within 600 ms.

Multi-device Collaboration. In office scenarios, multi-device collaboration often involves data transmission among a laptop-centered star network. For example, a smartphone might stream audio to both headphones and speakers while transferring files to other phones, where high data rates are crucial. Figure 16(b) compares the average goodput of SLE and BLE with varying numbers of connected peripherals. SLE maintains a rate of 2.15 Mbps, 4× that of BLE when two links in the network, which is still sufficient to support CD-level audio transmission between a smartphone and headphones.

6 Beyond Measurement

SLE's standard specifies a dynamic QoS control mechanism that monitors service performance during data transmission and, when necessary, adjusts QoS parameters and underlying link settings to maintain application requirements. To function effectively, this mechanism requires the ability to translate high-level QoS demands into concrete MAC- and PHY-layer parameter configurations adaptively. We address this need by designing a parameter optimisation framework that maps user-defined QoS priorities – such as goodput, latency, energy, and reliability – into an optimal set of configuration parameters under given constraints. This framework can be directly integrated with SLE's planned QoS management mechanism (as shown in Figure 11), enabling real-time parameter tuning and enhancing link adaptivity.

6.1 Design of Parameter Optimization

In short-range wireless communications, SLE offers highly configurable parameters, such as CI, BW, Txpower, and so on. However, the vast parameter space and diverse QoS requirements pose a major challenge. For example, HID devices prioritize end-to-end latency (<10 ms) over throughput, whereas audio streaming demands sustained high throughput (>2 Mbps). To address these varied requirements, this section proposes a parameter optimization design under multiple objectives, relying on experimental data to quantify the relationships between configuration parameters and application performance metrics. Furthermore, our design offers valuable guidance for implementing

cross-layer QoS coordination mechanisms and may inspire future research directions. The same optimisation process can be applied to BLE for selecting the best configuration for a given application profile, though the achievable benefits may be smaller due to its more limited parameter options and lack of dynamic QoS adjustment capability.

The sub-objective functions formulation methodology is first introduced according to the relationship model between parameters and metrics (Section 3.3) as follows:

$$\begin{aligned} &Energy = U \cdot (I_{Tx}T_{Tx} + I_{Rx}T_{Rx} + I_{IDLE}T_{IDLE})/CI, \\ &Good\,put = PL/CI \cdot (1 - BER)^{PL}, \\ &Latency = CI/2 + T_{Rx} + T_{Tx} + IFS, \\ &Reliability = PRR = (1 - BER)^{PL}, \end{aligned} \tag{2}$$

where $Energy$ is defined as the average consumption in one CI (Section 4.1), with U, I, T denoting voltage, current and duration respectively. $Good\,put$ is calculated as the product of theoretical throughput and corresponding PRR. $Latency$ is the approximated service latency (Section 4.3). $Reliability$ is defined as PRR (derived from BER and PL) same as that in $Good\,put$.

To integrate these four distinct metrics, we define a weighted objective function in which $\widehat{Good\,put}$, and so on. are the normalized values of $Good\,put$, and so on. to $[0,\ 1]$, as follows:

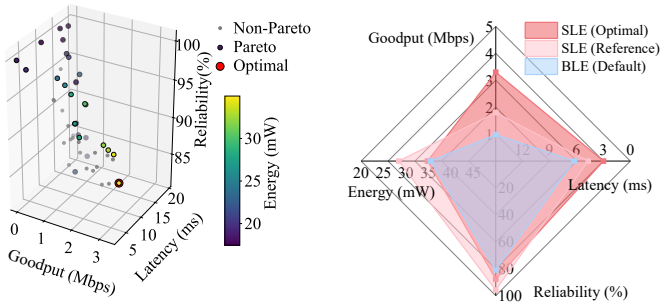
$$\begin{aligned} \min_{CI, P_{Tx}, BW, MCS, PL} \quad & -\Big(w_1 \cdot \widehat{Good\,put} + w_2 \cdot \widehat{Latency} \\ & + w_3 \cdot \widehat{Reliability} + w_4 \cdot \widehat{Energy}\Big), \\ s.t. \quad & CI > T_{Tx} + T_{Rx} + IFS + \Delta, \\ & Good\,put \geq a, \quad Latency \leq b, \\ & Reliability \geq c, \quad Energy \leq d. \end{aligned} \tag{3}$$

Equation (3) can serve as the core of the QoS management module as illustrated in Figure 11. Here, w_i ($i \in [1, 4]$) are adjustable weights that satisfy $w_1 + w_2 + w_3 + w_4 = 1$, and can be tuned according to different QoS requirements. The constraint on CI ensures that it exceeds the packet interaction time by a chipset-dependent delay Δ. Scenario-specific minimum QoS requirements are further represented by the constants a, b, c, and d.

When applied to the SLE QoS management module (Figure 11), application-layer QoS requirements are translated into weights (w_i) and constraints (a, etc.). For instance, in latency- and throughput-sensitive scenarios such as real-time gaming or other interactive applications, larger weights can be assigned to both w_1 (Goodput) and w_2 (Latency) to jointly guarantee high data rate and low delay. In contrast, for energy-constrained applications such as battery-powered IoT devices, assigning a higher weight to w_4 (Energy) emphasizes energy efficiency and helps extend device lifetime. The optimized output is then passed to the connection management module at the basic service layer, which establishes an appropriate transmission channel and configures the transmission parameters.

6.2 Example: Bulk Data Transfer

In this section, we adopt the designed parameters optimization for a scenario of file transfer to satisfy its QoS requirements. Specifically, we assign objective function weights to w_1=1.0, w_2=-0.5, w_3=0.2, w_4=-0.5, and impose performance constraints a=0, b=20 ms, c=0, d=35 mW, Δ=0.5 ms. The parameter space is further restricted by feasible ranges and standard design constraints such as $BW \in \{1, 2, 4\}\ MHz$, and so on. A reference solution to this discrete, nonlinear multi-objective



(a) Pareto frontier for bulk data transfer scenario

(b) Radar chart of BLE and SLE for bulk data transfer scenario

Fig. 17. (a) Pareto frontier and (b) radar chart for bulk data transfer scenario.

optimization problem is the elitist evolutionary algorithm NSGA-II [8], implemented via DEAP [13], which yields Pareto-optimal solutions delineating tradeoffs.

Figure 17(a) illustrates the generated Pareto frontier. From all non-dominated solutions, we select a goodput-prioritized optimal configuration as: BW=4 MHz, TxPower=-5.5 dBm, CI=1.8 ms, PL=817 bytes. Figure 17(b) compares three sample's performance of different configurations: a reference sample of SLE, the selected optimal sample of SLE, the default sample of BLE. The results show that the reference sample of SLE achieves balanced multi-objective performance. The generated solution for the case achieves better performance in terms of goodput, and completely dominates the default BLE parameters from the Android system [25], with BW=2 MHz, TxPower=4 dBm, CI=10 ms, PL= 244 bytes.

The conclusion drawn from this analysis is twofold. Firstly, it validates the feasibility of our proposed optimisation framework, demonstrating its capability to successfully identify a set of parameter configurations that satisfy application-layer QoS requirements. Secondly, it shows that protocols offering a richer and more flexible set of configurable MAC/PHY parameters, such as SLE in our test setup, can achieve greater optimization benefits.

7 Related Work

SparkLink Technology. Despite its technological significance, SparkLink (commonly known as NearLink) remains largely unexplored in academic research. In [15], the author introduces SparkLink's protocol features and application scenarios. However, none of studies have tested SparkLink's real performance using commercially available hardware, and the true performance characteristics of SparkLink remain largely unknown. This article is the first to conduct an in-depth evaluation of SparkLink's communication capabilities, revealing its real-world performance in short-range communication scenarios.

Bluetooth. A lot of works have been done to improve BLE's performance. For example, [17] reduces BLE's average latency of 20% by adopting time slotted channel hoping (which is used by Zigbee) on BLE's MAC layer. [28] improves TCP-over-BLE performance through adaptive connection event length adjustment, increasing TCP goodput by 101.6%. [38] improves BLE timeliness by estimating the number of connection events, reducing delayed packets by 40× in noisy RF environments. In addition to the communication capabilities, BLE 5.1 introduces **Angle of Arrival** (**AoA**) to expand its sensing capability based on phase difference measurement technology, enabling precise indoor positioning [6]. In contrast, our measurement study demonstrate SLE's exceptional communication

capabilities in terms of consumption, latency, throughput, and reliability. And SparkLink's official standard is also advancing toward a series of sensing capabilities, including AoA and **Time of Flight** (**ToF**) measurement, through a dedicated management module [1].

Measurement Study on Short Range Communication Technologies. [31] measures BLE's energy consumption, showing it outperforms ZigBee in energy efficiency per byte transferred. [16] measures the average power consumption and latency of BLE 4.0 with 24 bytes data. Studies [5, 9, 24, 41] measure the goodput of different BLE versions (BLE 4.0, BLE 5.0 coded, 1M/2M BLE 5.0) in service data exchange. [31] measures the relationship between RSSI and actual distance from beacons and smartphones. These studies fall short in providing detailed BLE current, goodput limit analysis, or a holistic assessment of advertising and scanning, resulting in an incomplete performance evaluation. In contrast, our work presents a rigorous and comprehensive analysis of BLE's performance at its boundaries, alongside a fair comparison with SLE.

8 Conclusion

This article is the first to offer a comprehensive benchmark of SLE's communication capabilities. We evaluate its performance in terms of power consumption, throughput, latency, and reliability, thereby demonstrating the improvements achieved by the underlying design. Our measurements show that SLE achieves a 4× increase in data rate, a 3.84× reduction in latency, and a 10 dB enhancement in sensitivity. We further validate these gains through end-to-end testing, confirming SLE's ability to meet diverse QoS requirements in real-world applications. Guided by experimental findings, we propose a parameter optimization design for a QoS coordination framework. While these findings demonstrate SLE's strong potential, we note that further considerations remain regarding hardware cost, coexistence with other wireless systems, and broader commercial availability. Addressing these aspects will enhance the maturity of the technology. Overall, our study provides valuable insights into this emerging platform and outlines a foundation for its future deployment and real-world impact.

References

[1] Sparklink Alliance. 2022. SparkLink Standards 1.0. Retrieved from https://sparklink.org.cn/en/standard/. Access data: 2025.10.1.

[2] Sparklink Alliance. 2022. SparkLink Wireless Communication System - Basic Service Layer - Device Discovery and Service Management No. T/XS 20001-2022. Retrieved from https://sparklink.org.cn/en/standard/view.php?id=7. Access data: 2025.10.1.

[3] Apple. 2024. Accessory Design Guidelines for Apple Devices. Retrieved from https://developer.apple.com/accessories/Accessory-Design-Guidelines.pdf. Access data: 2025.11.20.

[4] Takwa Attia, Martin Heusse, Bernard Tourancheau, and Andrzej Duda. 2019. Experimental characterization of packet reception rate in LoRaWAN. In *Rencontres Francophones sur la Conception de Protocoles, l'Évaluation de Performance et l'Expérimentation des Réseaux de Communication*.

[5] Andrea Aza, David Melendi, Roberto Garcia, Xabiel G. Paneda, Laura Pozueco, and Víctor Corcoba. 2022. Bluetooth 5 performance analysis for inter-vehicular communications. *Wireless Networks* 28, 1 (2022), 137–159.

[6] Bluetooth. 2019. Intro to New Features in Bluetooth Core Specification v5.1. Retrieved from https://www.bluetooth.com/bluetooth-resources/whats-new-in-bluetooth-5-1/. Access data: 2025.11.20.

[7] Leon Böttger, Alexander Matern, Dennis Arndt, and Matthias Hollick. 2025. Okay Google, where's my tracker? security, privacy, and performance evaluation of Google's find my device network. *Proceedings on Privacy Enhancing Technologies* 2025, 4 (2025), 606–619.

[8] K. Deb, A. Pratap, S. Agarwal, and T. Meyarivan. 2002. A fast and elitist multiobjective genetic algorithm: NSGA-II. *IEEE Transactions on Evolutionary Computation* 6, 2 (2002), 182–197.

[9] F. John Dian, Amirhossein Yousefi, and Sungjoon Lim. 2018. A practical study on bluetooth low energy (BLE) throughput. In *Proceedings of the 2018 IEEE 9th Annual Information Technology, Electronics and Mobile Communication Conference*. 768–771. DOI: 10.1109/IEMCON.2018.8614763

[10] ECC. 2024. ECC Report 356. Retrieved from https://docdb.cept.org/document/28607. Access data: 2025.11.20.

[11] ESnet. 2014. iPerf3: A TCP, UDP, and SCTP network bandwidth measurement tool. Retrieved from https://github.com/esnet/iperf. Access data: 2025.11.20.
[12] Espressif. 2024. ESP-IDF. Retrieved from https://www.espressif.com/en/products/sdks/esp-idf. Access data: 2025.11.20.
[13] Félix-Antoine Fortin, François-Michel De Rainville, Marc-André Gardner Gardner, Marc Parizeau, and Christian Gagné. 2012. DEAP: Evolutionary algorithms made easy. *Journal of Machine Learning Research* 13, 1 (2012), 2171–2175.
[14] USB Implementers Forum. 2025. USB HID. Retrieved from https://www.usb.org/hid. Access data: 2025.11.20.
[15] Mingjin Gao, Lei Wan, Rujing Shen, Yongqiang Gao, Jian Wang, Yonghui Li, and Branka Vucetic. 2023. SparkLink: A short-range wireless communication protocol with ultra-low latency and ultra-high reliability. *The Innovation* 4, 2 (2023), 1–3.
[16] Carles Gomez, Joaquim Oller, and Josep Paradells. 2012. Overview and evaluation of bluetooth low energy: An emerging low-power wireless technology. *Sensors* 12, 9 (2012), 11734–11753.
[17] Laura Harms and Olaf Landsiedel. 2023. TSCH meets BLE: Routed mesh communication over BLE. In *Proceedings of the 2023 19th International Conference on Distributed Computing in Smart Systems and the Internet of Things*. 187–195. DOI: 10.1109/DCOSS-IoT58021.2023.00041
[18] Wei He and M. Tariq Iqbal. 2024. A novel design of a low-cost SCADA system for monitoring standalone photovoltaic systems. *Journal of Electronics and Electrical Engineering* 3, 1 (2024), 107–116.
[19] HiSilicon. 2024. Hi2825v100. Retrieved from https://www.hisilicon.com/en/products/connectivity/short-range-IoT/nearlink-ble/Hi2825V100. Access data: 2025.11.20.
[20] HiSilicon. 2024.08. FBB-WS63. Retrieved from https://gitee.com/HiSpark/fbb_ws63. Access data: 2025.11.20.
[21] HiSilicon. 2025.08. FBB-BS2X. Retrieved from https://gitee.com/HiSpark/fbb_bs2x. Access data: 2025.11.20.
[22] Huawei. 2024. Huawei SLE wireless mouse. Retrieved from https://consumer.huawei.com/en/accessories/wireless-mouse-nearlink/. Access data: 2025.11.20.
[23] Haider Mahmood Jawad, Rosdiadee Nordin, Sadik Kamel Gharghan, Aqeel Mahmood Jawad, and Mahamod Ismail. 2017. Energy-efficient wireless sensor networks for precision agriculture: A review. *Sensors* 17, 8 (2017), 1781.
[24] Heikki Karvonen, Carlos Pomalaza-Ráez, Konstantin Mikhaylov, Matti Hämäläinen, and Jari Iinatti. 2019. Experimental performance evaluation of BLE 4 versus BLE 5 in indoors and outdoors scenarios. In *Proceedings of the Advances in Body Area Networks I: Post-Conference Proceedings of BodyNets 2017*. Springer, 235–251.
[25] Tong Li, Jiaxin Liang, Yukuan Ding, Kai Zheng, Xu Zhang, and Ke Xu. 2023. On design and performance of offline finding network. In *Proceedings of the IEEE INFOCOM 2023 - IEEE Conference on Computer Communications*. 1–10. DOI: 10.1109/INFOCOM53939.2023.10228880
[26] Logitech. 2025. Mouse. Retrieved from https://www.logitechg.com/zh-cn/products/gaming-mice.html
[27] Jiamei Lv, Wei Dong, Yi Gao, and Chun Chen. 2022. Performant TCP over BLE. In *Proceedings of the 2022 IEEE 30th International Conference on Network Protocols*. 1–11. DOI: 10.1109/ICNP55882.2022.9940406
[28] Jiamei Lv, Wei Dong, Yi Gao, and Chun Chen. 2022. Performant TCP over BLE. In *Proceedings of the 2022 IEEE 30th International Conference on Network Protocols*. 1–11. DOI: 10.1109/ICNP55882.2022.9940406
[29] Luca Negri, J. Beutel, and Matthias Dyer. 2006. The power consumption of Bluetooth scatternets. *CCNC 2006. 2006 3rd IEEE Consumer Communications and Networking Conference, 2006.* 1 (2006), 519–523.
[30] Mohamad Omar Al Kalaa, Walid Balid, Naim Bitar, and Hazem H. Refai. 2016. Evaluating bluetooth low energy in realistic wireless environments. In *Proceedings of the 2016 IEEE Wireless Communications and Networking Conference*. 1–6. DOI: 10.1109/WCNC.2016.7564809
[31] Jeongyeup Paek, JeongGil Ko, and Hyungsik Shin. 2016. A measurement study of BLE iBeacon and geometric adjustment scheme for indoor location-based mobile applications. *Mobile Information Systems* 2016, 1 (2016), 8367638.
[32] Panasonic. 2024. CR2032. Retrieved from https://energy.panasonic.com/na/business/products/lithium/models/CR2032. Access data: 2025.11.20.
[33] Nordic Semiconductor. 2024. nRF5 SDK v17.1.0. Retrieved from https://docs.nordicsemi.com/bundle/sdk_nrf5_v17.1.0/page/index.html. Access data: 2025.11.20.
[34] Nordic Semiconductor. 2025. Device Firmware Update. Retrieved from https://www.nordicsemi.cn/blog/bluetooth-over-the-air-upgrade-ota/. Access data: 2025.11.20.
[35] Bluetooth Special Interest Group (SIG). 2016.12. Bluetooth Core Specification 5.0. Retrieved from https://www.bluetooth.com/specifications/specs/core-specification-5-0/. Access data: 2025.11.20.
[36] Bluetooth Special Interest Group (SIG). 2024.10. The Bluetooth Low Energy Primer. Retrieved from https://www.bluetooth.com/bluetooth-le-primer/. Access data: 2025.11.20.
[37] Japan Audio Society. 2022.11. Definition of Hi-Res Audio. Retrieved from https://www.jas-audio.or.jp/english/hi-res-logo-en. Access data: 2025.11.20.
[38] Michael Spörk, Carlo Alberto Boano, and Kay Römer. 2020. Improving the timeliness of bluetooth low energy in dynamic rf environments. *ACM Trans. Internet Things* 1, 2 (2020), 32 pages. DOI: 10.1145/3375836

[39] USB. 2024. Human Interface Devices (HID) Specifications and Tools. Retrieved from https://www.usb.org/hid. Access data: 2025.11.20.
[40] Junjie Yin, Zheng Yang, Hao Cao, Tongtong Liu, Zimu Zhou, and Chenshu Wu. 2019. A survey on bluetooth 5.0 and mesh: New milestones of IoT. *ACM Transactions on Sensor Networks* 15, 3 (2019), 29 pages. DOI: 10.1145/3317687
[41] Junjie Yin, Zheng Yang, Hao Cao, Tongtong Liu, Zimu Zhou, and Chenshu Wu. 2019. A survey on Bluetooth 5.0 and mesh: New milestones of IoT. *ACM Transactions on Sensor Networks* 15, 3 (2019), 1–29.

Received 5 June 2025; revised 21 September 2025; accepted 22 September 2025